JOURNAL OF SOLID STATE CHEMISTRY 43, 107–125 (1982)

Structure Types and Phase Transformations in $KMnCl_3$ and $TlMnCl_3$

A. HOROWITZ,* M. AMIT, AND J. MAKOVSKY

Nuclear Research Center–Negev, P.O.B. 9001, Beer Sheva, Israel

AND L. BEN DOR, AND Z. H. KALMAN

Hebrew University of Jerusalem, Jerusalem, Israel

Received September 18, 1981; in revised form February 16, 1982

$KMnCl_3$ and $TlMnCl_3$ are known to crystallize in tetragonal and cubic perovskite structures, respectively. Room temperature X-ray diffraction data obtained in our laboratory proved that the perovskite structure of $KMnCl_3$ is orthorhombic. The space group is *Pnma* and $Z = 4$. Unit cell parameters are $a = 7.08(1)$, $b = 9.97(1)$, and $c = 6.98(1)$ Å. Experimental data showed that the perovskite structures of $KMnCl_3$ and $TlMnCl_3$ are not stable, and that both materials transform slowly into another orthorhombic, nonperovskite $KCdCl_3$ structure with space group *Pnma* and $Z = 4$. Cell parameters of these structures are $a = 8.769(7)$, $b = 3.883(9)$, and $c = 14.42(1)$ Å for $KMnCl_3$ and $a = 8.926(8)$, $b = 3.839(9)$, and $c = 14.77(1)$ Å for $TlMnCl_3$. The nonperovskite structures of $KMnCl_3$ and $TlMnCl_3$ transform on heating to the perovskite structures and these phase transitions are not immediately reversed. No correlation could be found between the $KCdCl_3$ structure and water incorporation in the crystal lattice as has been previously suggested. An analysis of the factors that cause the K structure to be exhibited in chloride and to be absent in the fluoride compounds is also presented.

1. Introduction

The crystal structures of the different $ABCl_3$ (A = alkali metal, NH_4, or Tl, B = divalent metal) compounds were investigated by several research groups (e.g., 1–4) and attempts were made to analyze the factors that cause some of these compounds to crystallize in a manner different from their parallel fluoride compounds (*5–12*). Special attention is drawn to the obvious preference of the double chloride perovskites (P phases) to a hexagonal rather than cubic stack of their ACl_3 close-packed layers. The existence of the nonperovskite $KCdCl_3$ (K) structures (and their absence in ABF_3 fluorides) drew less attention. Until recently, five $ABCl_3$ compounds, all with Cd or Hg, were known to crystallize in this structure: $KCdCl_3$ (*3*), NH_4CdCl_3 (*13*), $RbCdCl_3$ (*13*), $TlHgCl_3$ (*14*), and $NaHgCl_3$ (*15*). These compounds were referred to as "exceptions" (*12*) and it was suggested that their structure was somehow connected to the existence of water in the crystal lattice (*4*). The relation between the K structure and the polarizability of the B cations was also pointed out (*5, 12*).

Recently, four new Cr and Cu $ABCl_3$ (A = K, Tl) compounds were reported to crystallize in the $KCdCl_3$ structure with an additional cooperative Jahn–Teller distortion (*16*). Our investigation of the ACl–BCl_2 systems (with B = Mn, Fe, Co, Ni) revealed

* Author to whom correspondence should be addressed.

0022-4596/82/080107-19$02.00/0

three new chloride compounds with the K structure. In a previous paper we reported on the crystal structure of $KFeCl_3$ (and $KFeBr_3$) (*17*), and this paper reports on the K phases of $KMnCl_3$ and $TlMnCl_3$. $KMnCl_3$ and $TlMnCl_3$ have been known to crystallize in tetragonal (*1*) and cubic (*2*) P phases. Both materials were previously prepared from molten salts.

Our experiments with $KMnCl_3$ and $TlMnCl_3$ revealed that the P structure of $KMnCl_3$ is orthorhombic rather than tetragonal and that the P phases of $KMnCl_3$ and $TlMnCl_3$ transform at room temperature very slowly into the K phases. On heating, the K phases transform into the P phases and these phase transformations are not immediately reversed.

Former reports about the P phases of $KMnCl_3$ and $TlMnCl_3$ indicate a few thermal effects. Croft *et al.* (*1*) reported on a melting point of 507 ± 5°C for $KMnCl_3$ and a phase transformation from a tetragonal to cubic structure at 450°C. Seifert and Koknat (*18*) reported on a somewhat lower melting point (490°C) for this material and on a phase transformation at 386°C. Previous investigations on $TlMnCl_3$ show that this material has a cubic P phase at room temperature (*2*) and that distortions to lower symmetries occur at lower temperatures (*19, 20*). A melting point of 497°C was reported for $TlMnCl_3$ (*21*).

The P and K phases of $KMnCl_3$ were recently investigated in our laboratory by neutron diffraction to examine the relation between the magnetic and crystallographic properties in these materials (*22, 23*).

2. Experimental

2.1. Material Preparation

The P phases of $KMnCl_3$ and $TlMnCl_3$ were prepared by melting a stoichiometric mixture of dried KCl (Merck suprapure) or TlCl (Koch Light 8721P) with $MnCl_2$ in evacuated and sealed quartz ampoules. The anhydrous $MnCl_2$ was prepared by heating $MnCl_2 \cdot 4H_2O$ (Merck G.R.) in a dried HCl stream. (60–80 g of $MnCl_2 \cdot 4H_2O$ were heated in three stages: ~2 hr at 110–130°C; ~2 hr at 180–200°C; and ~3 hr at 250–280°C. The temperature was raised from one stage to the next only after water or water vapor was no longer detected at the exhaust of the reaction tube.) TlCl and KCl were dried for 4–8 hr in a vacuum furnace. The heating temperatures were 100–120°C for TlCl and ~250°C for KCl.

X-Ray examination of these materials after storage in evacuated (10^{-6}) and sealed glass ampoules for 3.5–4.5 years revealed partial transformation of the materials to the K phases. Different samples exhibited different amounts of partial transformation. Examination of fresher materials revealed that in some samples, the transformation to the K phase began after ~3 weeks, although very slight amounts (~5%) of the K phase were detected in these cases. Examinations of different samples revealed that the amount of the material being transformed into the K phase increased with the amount of grinding of the materials, although this relationship was not established quantitatively.

The K phase of $KMnCl_3$ was prepared by several techniques (*24*), of which the following one was found to be very convenient: a 1 : 2 molar ratio mixture of KCl and $MnCl_2 \cdot 4H_2O$ (respectively) was dissolved in a minimal amount of water acidified with a few HCl drops. Slow evaporation of the solution yielded $KMnCl_3 \cdot 2H_2O$ crystalline needles (*25*). K $KMnCl_3$ powder was produced by drying the needles at 90°C in vacuum.

Several experiments aimed at the preparation of the K phase of $TlMnCl_3$ from water or alcoholic solutions did not succeed: a mixture of the constituent materials with or without P $TlMnCl_3$ was obtained (*24*). Also, the dehydration of hydrated $TlMnCl_3$ at low

temperatures (~90°C) yielded the cubic P phase. All the K phase $TlMnCl_3$ samples for the experiments described below were therefore obtained by the spontaneous slow transformation of the powdered P $TlMnCl_3$ material.

Chemical analysis of the manganese ions was carried out by an EDTA titration and that of the chloride ions by an argentometric titration. The results of the analysis of the different materials were in good agreement with the expected calculated values.

Because of the highly hygroscopic nature of anhydrous $MnCl_2$, $KMnCl_3$, and $TlMnCl_3$, all weighings and sample preparations were carried out under dry argon atmosphere.

The density of the P phase of $KMnCl_3$ was determined by the immersion method, using *n*-dodecane as a solvent. The densities of the K phases were not determined experimentally because of the powdered nature of the materials.

2.2. *X-Ray Techniques*

Cell dimensions of the different phases were determined from Guinier–De Wolff powder photographs (effective camera radius 114.6 mm) using Cu $K\alpha$ radiation with a Ni foil placed in contact with the film to reduce fluorescence background. For calibration purposes, a small amount of KCl was added to some samples. The samples for the Guinier–De Wolff measurements were prepared by a homogeneous dispersion of fine-ground powder on a sheet of an adhesive tape placed on the window of the sample holder. This way of preparation prevented preferred crystal orientation. Cell dimensions were determined by using a least-squares computer program (*26*) which produced the best fit between calculated and observed *d* values.

Powder pattern intensities were measured on a PW 1050 Philips diffractometer with a NaI(Tl) detector and an INS-11 Elscint electronic system. Relative observed intensities were determined from the areas under the diffraction peaks above background. For the relative error (ΔN) of each reflection, the relation $\Delta N = N^{1/2}$ was assumed, where N is the total number of counts under each peak. Calculations of relative intensities (I) were carried out by using $I \alpha m LPF^2$, where m is the multiplicity factor, LP the Lorenz polarization factor, and F the structure factor. Structure factors were calculated using H.S.F. atomic structure factors (*27*), corrected for anomalous dispersion. No temperature or absorption corrections were applied. Atomic positions giving the best fit between observed and calculated intensities were found by using a least-squares computer program (*28*), minimizing the residual R factor $\{R = [\Sigma(I_o - I_c)^2]^{1/2}/(\Sigma I_o^2)^{1/2}\}$. To prevent errors arising from preferred orientation, the diffractometer powder patterns were compared to the Guinier–De Wolff photographs to ensure identical relative intensities. For the determination of the crystal structure, only pure K $TlMnCl_3$ samples were used.

To prevent hydration, both the Guinier–De Wolff camera and the diffractometer systems were evacuated during exposure and contained a drying agent.

2.3. *Examination of Phase Transformations*

The K → P phase transformation temperatures of $KMnCl_3$ and $TlMnCl_3$ were established through heat treatment experiments in which a few grams of the materials were heated in dynamic vacuum or in vacuum-sealed ampoules at different temperatures for prolonged periods (3–166 hr). The $KMnCl_3$ samples consisted of a pure K phase material prepared from aqueous solutions, while most of the $TlMnCl_3$ samples contained about 50% of the cubic P phase as revealed by an X-ray analysis prior to the heat treatment experiments. Since the reversed P → K transformation could not be detected before at least a few weeks of

shelf life, it was possible to determine the K → P transformation temperatures by establishing the temperatures of the heat treatments that yielded a P phase via an X-ray examination of the different samples after the treatments. The relative amounts of the K and P phases in the different samples and end products were estimated from the relative intensities of the respective X-ray diffraction lines of these two phases. Care was taken during the heat treatment experiments to ensure a minimum distance between the temperature-measuring thermocouple and the heated samples. Additional measurements with a calibrated mercury thermometer immersed in the sample material revealed temperature inhomogeneities of less than 5°C.

Careful weighing of some of the samples before and after the heat treatment revealed the occurrence of weight losses as small as 0.01% during the heat treatment.

The temperature and the nature (endothermic or exothermic) of the different thermal effects occurring on heating $KMnCl_3$ and $TlMnCl_3$ samples were determined by the differential scanning calorimeter (DSC) of a thermal analyzer (DuPont Model 990). Since considerable evaporation (and probably decomposition and/or chemical reactions) occurred at high temperatures ($t >$ 400°C) when open sample holders were used, these experiments were carried out with press-sealed, gold-plated sample holders. Visual observation proved, however, that with the $TlMnCl_3$ samples, some reaction(s) occurred with these sample holders above 400°C. The $TlMnCl_3$ samples were therefore additionally wrapped in gold foils. Care was taken to wrap the samples as "hermetically" as possible with the gold foil and the reference sample holder contained approximately the same amount of gold foil. Under these conditions, some of the $TlMnCl_3$ samples still exhibited slight reaction with the sample holder above 400°C.

3. Results

3.1. Crystal Structures

3.1.1. P $KMnCl_3$. The P $KMnCl_3$ Guinier–De Wolff photographs that were carried out at our laboratory revealed a few diffraction lines that were not detected by Croft *et al.* (*1*). These lines were not compatible with the former proposed tetragonal structure and it was possible to index all the lines in the orthorhombic system with a = 7.08(1), b = 9.97(1), and c = 6.98(1) Å. The measured density (2.69(3) g/cm³) is in good agreement with four molecules per unit cell (calculated density: 2.70 g/cm³). Intensity measurements were carried out by the diffractometer. Because of the lower resolving power, only the total intensities of the unresolved lines could be measured.

Good fit between observed and calculated intensities were obtained by assuming the space group *Pnma* with the following atomic positions:

K in (4*c*) with x = 0.055(6),	y = 0.25,	z = 0.991(8),
Mn in (4*b*) with x = 0,	y = 0,	z = ½,
Cl_I in (4*c*) with x = 0.51(1),	y = 0.25,	z = 0.039(7),
Cl_{II} in (8*d*) with x = 0.30(1),	y = 0.041(3),	z = 0.71(1).

Although the calculated R is low (R = 0.042), this does not indicate a small error in the atomic positions but a low sensitivity of R to changes in the integral intensities (because of the unresolved lines) and a relatively small number of observed lines (~ 11 lines).

The structure is derived from the perovskite structure when $a_{orth} \approx 2^{1/2}\, a_{cub}$, $b_{orth} \approx 2a_{cub}$, and $c_{orth} \approx 2^{1/2}\, a_{cub}$. This

TABLE I

RESULTS OF HEAT TREATMENT EXPERIMENTS WITH $KMnCl_3$ AND $TlMnCl_3$

Starting material	Temperature of heat treatment (°C)	Duration of heat treatment (hr)	Percentage of evaporated material	End product
$KMnCl_3 \cdot 2H_2O$	86	17		K
$KMnCl_3 \cdot 2H_2O$	89–93	72		K
K $KMnCl_3$	152	18	0.032	K:P 10:1
K $KMnCl_3$	160	60		K
K $KMnCl_3$	169	3	0.468	K
K $KMnCl_3$	169	3	0.000	K:P 10:1
K $KMnCl_3$	180	18		K:P 10:1
K $KMnCl_3$	192	18		K:P 10:1
K $KMnCl_3$	198	18		K:P 10:4
K $KMnCl_3$	190–198	72	1.24	K:P 5:10
K $KMnCl_3$	190–198	72	0.000	P
K $KMnCl_3$	190–198	26	0.075	K:P 1:10
K $KMnCl_3$	204	18	0.050	K
K $KMnCl_3$	206	48		K:P 8:10
K $KMnCl_3$	207	18		K
K $KMnCl_3$	213–219	9		K:P 1:10
K $KMnCl_3$	232	18		K:P 3:10
K $KMnCl_3$	260	18		P
K $KMnCl_3$	263	20		P
K $KMnCl_3$	270	18		K + P
$TlMnCl_3$ K:P 1:1	88	166		K:P 1:1
K $TlMnCl_3$	89	32		K:P 10:1
K $TlMnCl_3$	92	18		K
$TlMnCl_3$ K:P 1:1	125–129	43		K:P 1:1
$TlMnCl_3$ K:P 1:1	144	66		K:P 2:10
$TlMnCl_3$ K:P 1:1	168	46		P
$TlMnCl_3$ K:P 1:1	249	46		P
K $TlMnCl_3$	220–260	18		P
$TlMnCl_3$ K:P 1:1	249	46		P
$TlMnCl_3$ K:P 1:1	355	45		P

Note. The relative amounts of the K and P phases in the starting materials and in the end products were estimated from the relative intensities of the respective diffraction lines in the Guinier–De Wolff photographs.

structure was previously described for $KMgCl_3$ (*29*).

Observed and calculated *d* values and intensities are given in Table II, together with the former data of Croft *et al.* (*1*). These results are in good agreement with the results obtained by neutron diffraction studies (*23*).

3.1.2. *K $KMnCl_3$ and $TlMnCl_3$.* These phases were found to crystallize in the orthorhombic structure with $a = 8.769(7)$, $b = 3.883(9)$, $c = 14.42(1)$ Å for $KMnCl_3$ and

TABLE II

CALCULATED AND OBSERVED *d* VALUES AND INTENSITIES FOR P $KMnCl_3$. A COMPARISON WITH THE DATA OF CROFT *et al.* (*1*)

Our data					Croft *et al.*			Our data					Croft *et al.*		
hkl	d_{cal}	d_{obs}	I_{cal}	I_{obs}[a]	d_{obs}	I_{obs}[a]	*hkl* (Tet)	*hkl*	d_{cal}	d_{obs}	I_{cal}	I_{obs}[a]	d_{obs}	I_{obs}[a]	*hkl* (Tet)
011	5.718		3	n.o.[b]				301	2.236				2.236	w	024, 240, 402
020	4.985	4.995	42	42	5.007	m+	200,002	141	2.228	2.233					
101	4.971							222	2.224		30	29			
111	4.448		1	n.o.[b]				103	2.210	2.208					
200	3.548	3.566						311	2.182	2.188					
121	3.520	3.520	56	54	3.537	m	220, 202	113	2.158		2	n.o.			
002	3.490	3.514						321	2.040	2.041			2.043	m	422
210	3.336		3	n.o.[b]				240	2.038		43	45			
201	3.157	3.146	12	9				042	2.028	2.031			2.031	m−	224
102	3.130	3.129						123	2.021						
211	3.010	3.015	21	18	3.015	w	311, 133	232	1.990		<1	n.o.			
031	3.001							241	1.956		1	n.o.			
112	2.987	2.998						302	1.955		1	n.o.			
220	2.886	2.885	35	34	2.981	s−	222	142	1.950		<1	n.o.			
022	2.859	2.866						203	1.944		1	n.o.			
131	2.763	2.769	4	2	2.778	w	203, 320, 302	312	1.918		<1	n.o.			
221	2.667	2.665	12	11	2.680	w	321, 132	051	1.917		4	n.o.			
122	2.651	2.657			2.665	w	123	213	1.908		<1	n.o.[b]			
040	2.493	2.503	100	100	2.506	s	400	033	1.906		<1	n.o.[b]			
202	2.485	2.489						331	1.855		1	n.o.[b]			
230	2.423	2.420	7	5[c]				151	1.851		<1	n.o.[b]			
212	2.412	2.410	6	5[c]				133	1.841		1	n.o.[b]			
231	2.289		4	n.o.				322	1.820		<1	n.o.[b]			
132	2.279		1	n.o.				223	1.811		1	n.o.[b]			
013	2.266		2	n.o.				400	1.770	1.778					
								242	1.760	1.765	43	43	1.767	m	440, 404
								004	1.745	1.754					

[a] The intensities were measured using the diffractometer. Because of lower resolving power, the total intensities of these unresolved lines were measured.

[b] These lines were not observed in our powder diffraction data and were introduced with intensity 5 (the noise intensity) into the computer program.

[c] These lines were not observed by the diffractometer. The relative intensities were estimated from the Guinier–De Wolff photographs.

$a = 8.926(8)$, $b = 3.839(9)$, $c = 14.77(1)$ Å for $TlMnCl_3$. Because of the powdered nature of the materials, density measurements were not carried out.

Best fit between calculated and observed intensities were obtained by assuming a (nonperovskite) *Pnma* space group with $Z = 4$ and the following atomic positions (all atoms in 4*c* positions with x, $\frac{1}{4}$, z).

$KMnCl_3$:

K with $x = 0.433(5)$, $z = 0.828(4)$,
Mn with $x = 0.175(6)$, $z = 0.056(3)$,
Cl_I with $x = 0.273(5)$, $z = 0.213(5)$,
Cl_{II} with $x = 0.012(5)$, $z = 0.902(4)$,
Cl_{III} with $x = 0.163(8)$, $z = 0.500(4)$,
$R = 0.06$;

$TlMnCl_3$:

Tl with $x = 0.438(2)$, $z = 0.825(2)$,
Mn with $x = 0.169(7)$, $z = 0.058(8)$,
Cl_I with $x = 0.277(14)$, $z = 0.209(12)$,
Cl_{II} with $x = 0.022(17)$, $z = 0.890(8)$,
Cl_{III} with $x = 0.187(13)$, $z = 0.485(9)$,
$R = 0.08$.

The higher error in the atomic positions of the chlorine atoms arises from the fact that Tl is the heaviest atom and small changes in the atomic positions of the lighter atoms do not change the calculated intensities significantly.

Calculated and observed *d* values and intensities of K $KMnCl_3$ are given in Table III and those of K $TlMnCl_3$ are given in Table IV. The results on $KMnCl_3$ are in good agreement with the results obtained by neutron diffraction studies (*22*).

3.2. Phase Transformations

The results of the heat treatment experiments are given in Table I and those of the DSC analysis are presented in Figs. 1 and 2. The thermal effects exhibited by the sam-

TABLE III

CALCULATED AND OBSERVED *d* VALUES AND INTENSITIES FOR K $KMnCl_3$[a]

hkl	d_{cal}	d_{obs}	I_{cal}	I_{obs}	*hkl*	d_{cal}	d_{obs}	I_{cal}	I_{obs}
101	7.489	7.518	11	15	313	2.100	2.100	3	4
002	7.209	7.239	27	30	402	2.097		4	
102	5.569	5.577	25	21	215	2.047	2.050	2	1
103	4.215	4.218	7	18	107	2.005	2.000	5	7
201	4.195		11		403	1.995	1.991	8	20
111	3.447	3.449	17	18	116	1.990		6	
104	3.334	3.337	8	6	314	1.960	1.959	29	30
203	3.239	3.242	10	9	020	1.942	1.940	29	31
210	2.907	2.903	8	9	410	1.909	1.907	11	13
113	2.856	2.851	22	100	207	1.864	1.863	5	6
211	2.850		78		412	1.845	1.844	9	10
204	2.785	2.786	30	29	122	1.833	1.830	2	2
105	2.740	2.740	33	36	117	1.782	1.782	21	20
302	2.709	2.711	15	86	413	1.774	1.772	10	10
212	2.696	2.696	72		405	1.745	1.744	6	7
114	2.530	2.526	6	5	501	1.741		3	
213	2.487	2.488	7	8	502	1.704	1.700	3	2
106	2.318	2.316	14	40	118	1.607	1.598	8	15
015	2.315		24		224	1.593		8	
304	2.270	2.271	6	14	125	1.584	1.585	10	10
214	2.263		8		322	1.578	1.580	5	4
312	2.222	2.220	12	15					

[a] The intensities were measured using the diffractometer.

TABLE IV

CALCULATED AND OBSERVED d VALUES AND INTENSITIES FOR K T1MnCl$_3$

hkl	d_{cal}	d_{obs}	I_{cal}	I_{obs}	hkl	d_{cal}	d_{obs}	I_{cal}	I_{obs}
101	7.640	7.685	14	15[a]	216	1.880	1.880	10	10
002	7.386	7.443	13	15[a]	121	1.862	1.860	1	3
102	5.691	5.750	2	3	022	1.858		1	
200	4.463	4.457	8	8	017	1.849	1.849	2	6
103	4.312	4.318	61	72	008	1.847		4	
201	4.272	4.267	34	40	315	1.840	1.842	5	5
202	3.820	3.817	15	14	117	1.811	1.811	3	6
011	3.716	3.715	31	33	108	1.808		1	
111	3.430	3.431	9	10	413	1.796	1.796	2	2
104	3.413	3.412	7	7	405	1.781	1.782	8	6
112	3.182	3.178	33	33	220	1.763	1.763	2	2
210	2.910	2.901	4	2	123	1.754	1.754	12	18
113	2.867	2.862	22		221	1.751		6	
211	2.855	2.851	65	100	502	1.735	1.734	7	6
204	2.845	2.847	13		222	1.715	1.718	3	4
105	2.805	2.801	29	40	217	1.708	1.708	8	9
302	2.760	2.757	24	32	208	1.706		1	
212	2.708	2.704	36	42	118	1.636	1.636	6	8
114	2.551	2.547	31	32	109	1.614	1.615	4	2
303	2.547		2		224	1.591	1.590	4	2
205	2.464	2.460	1	9	125	1.584	1.585	10	13
006	2.462		8		512	1.581		2	
106	2.373	2.370	1	1	322	1.576		9	
015	2.341	2.339	26	30	317	1.571	1.576	1	10
311	2.322	2.317	9	27	308	1.569		1	
304	2.317		18		218	1.559	1.559	3	3
214	2.286	2.283	3	5	513	1.538		12	
401	2.206	2.204	11	10	407	1.533	1.533	4	17
206	2.156	2.156	6	5	323	1.533		1	
313	2.122	2.122	17	16	416	1.519		10	
215	2.073	2.078	3	3	225	1.514	1.516	1	12
403	2.033	2.033	4	2	026	1.514		4	
116	2.019	2.020	6	6	119	1.488	1.488	3	5
314	1.984	1.985	12	14	514	1.483		2	
410	1.929	1.930	16	16	601	1.480	1.480	1	11
020	1.920	1.921	17	18	324	1.478		9	
207	1.908	1.908	9	9	602	1.458	1.457	3	3

[a] These intensities were measured from Guinier–De Wolff photographs. All other intensities were measured using the diffractometer.

ples during the DSC analyses are presented in Sections 3.2.1 and 3.2.2 by an indication of their temperatures in °C. Exothermic effects are given in parentheses. The serial numbers of the samples are designated by Roman numerals, while the first, second, and third heating cycles are designated by a, b, and c, respectively. The same designations are also used in Figs. 1 and 2. Thermal effects with very very small intensities which were not exhibited by several samples are designated by vvs.

3.2.1. $KMnCl_3$. The heat treatment experiments of $KMnCl_3$ samples revealed that no K → P phase transformation occurred with these samples below 90°C. Between

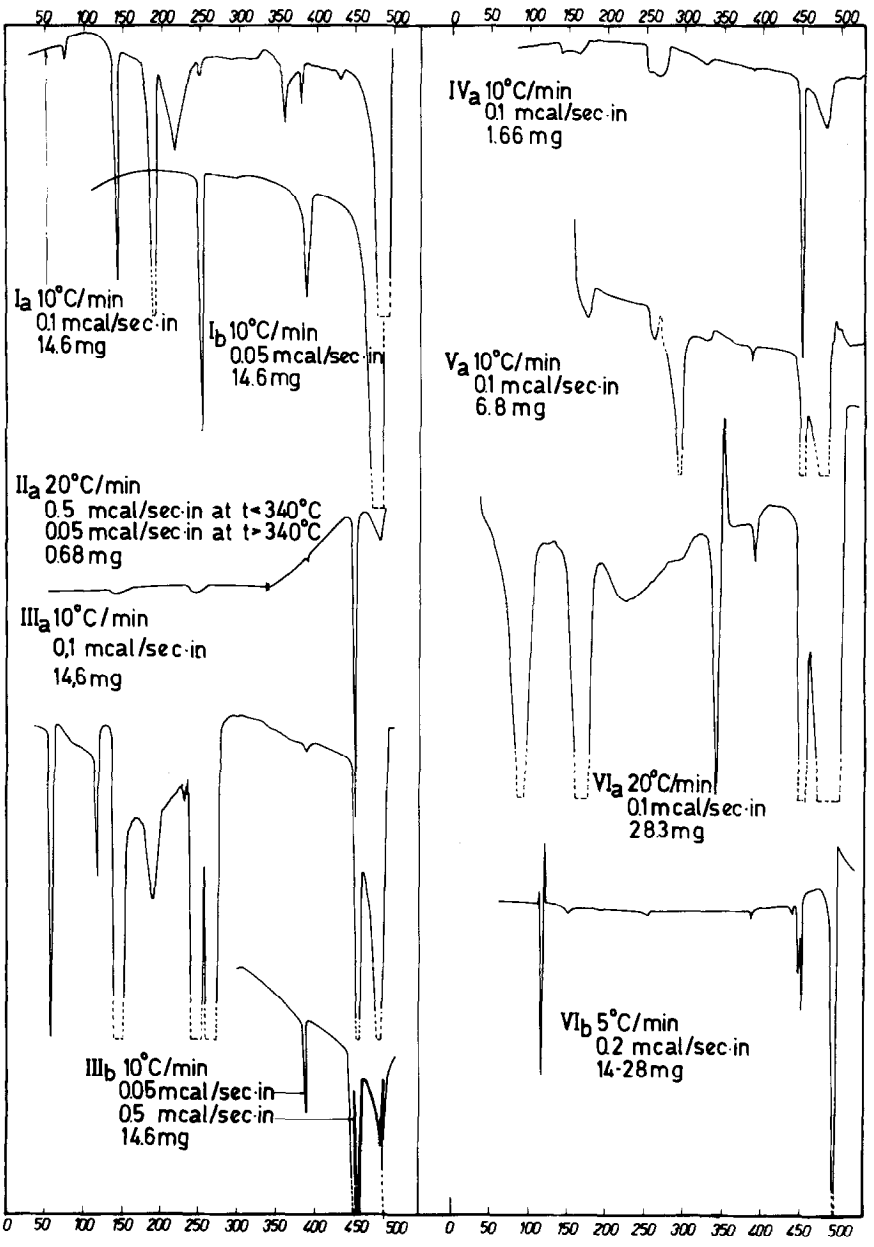

FIG. 1. DSC analysis of $KMnCl_3$ samples. I–VI: serial numbers of the samples (see text); a and b designate first and second heating cycles, respectively.

150 and 230°C, different K $KMnCl_3$ samples exhibited different amounts of partial transformation to the P phase. It seems that with higher temperatures of the heat treatment more material transformed into the P phase, although some samples did not follow this pattern of behavior. Below 190°C only slight amounts of the material transformed into the P phase.

Six different $KMnCl_3$ samples were analyzed by the DSC attachment of the thermal analyzer and the following thermal effects

were detected (Fig. 1):

I_a	K phase	75			143			190	220	252		295			360	383	430	490
II_a	P phase (+ K phase?)				145					250						386	445	495
III_a	K + P phases	58		117		145			190	233	250	265				383	450	480
IV_a	K + P phases				135		160				255	270		330		386	450	480
V_a	K + P phases							175			260		295	330		386	450	475
VI_a	K + P phases		87				165			225			295	340(345)		386	450	487

In repeated heating cycles (performed immediately after the first heating cycle) the following thermal effects were detected (Fig. 1):

I_b										253						386		475
I_c	Not shown in Fig. 1, the heating began at 300°C															385	450	475
III_b	The heating began at 300°C															385	450	470
																	438	
VI_b				115		150				255						386	445	486
				(118)		vvs											450	

Sample I was a K phase prepared from aqueous solutions, and samples II–V were prepared from molten salts. Sample II was a few weeks old, while III–V were a few months old. Sample VI was a K phase material prepared from aqueous solutions that was heated a few hours at 270°C 3 days before the DSC analysis. The X-ray pattern of this sample revealed that it consisted of both the K and the P phases. The DSC analysis of sample VI was carried out in an open gold-plated aluminum sample holder and the weighing of this sample after two subsequent runs revealed a weight loss of about 14 mg. The 345°C exothermic effect of this sample on the first heating cycle is probably connected with some sort of chemical reaction, as are probably the low-temperature (t < 255°C) effects and the triple effect (at ~450°C) on the second heating cycle of sample VI.

Visual estimation indicates that the intensity of the thermal effect at 255°C increased on the second heating cycle relative to the first one (sample I) and that the relative intensities of the last two thermal effects (~450 and ~480°C) rise and fall at the expense of each other. It is supposed that an overheated state of the material is possible for the effect at 450°C (second heating cycle of sample I). The results from the heat treatment experiments (Table I) indicate that the thermal effects that were exhibited below 90°C were probably connected to water evaporation.

The DSC analysis of $KMnCl_3$ reveals that the four thermal effects detected in the second heating cycles (255, 386, 450, and 475–490°C) are all exhibited by the P $KMnCl_3$. The three higher-temperature effects are in agreement with the 490°C melting point and the 386°C phase transformation reported by Seifert *et al.* (*18*) and with the 450°C tetragonal → cubic phase transformation reported by Croft *et al.* (*1*). The 255°C effect is reported herein for the first time.

The other thermal effects (t > 90°C) detected on the first heating cycles of $KMnCl_3$ samples, and especially the fact that different thermal effects were exhibited by differ-

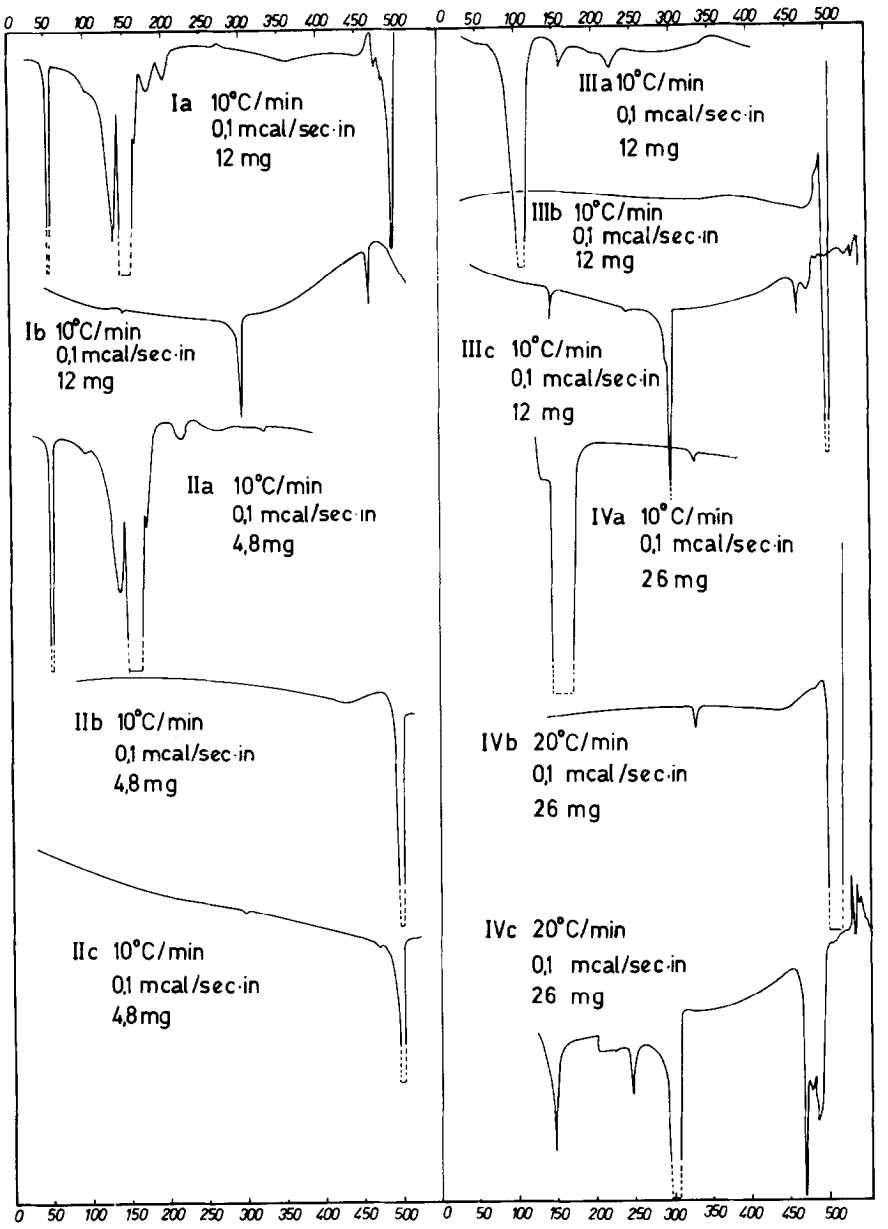

FIG. 2. DSC analysis of $TlMnCl_3$ samples. I–IV: serial numbers of the samples; a, b, and c designate first, second, and third heating cycles, respectively.

ent samples, indicate that the K → P phase transformation proceeds by more than one pathway. The possibility that some of these effects are connected to water vaporization and/or to chemical reactions (although such reactions were not visually observed in samples I–V) cannot be excluded. However, the conclusion that different pathways exist for the K → P phase transformation is sufficiently supported by the results of the

heat treatment experiments where only partial K → P phase transformation occurred in K samples heated between 150 and 270°C. Temperature inhomogeneities over the heated samples cannot be the cause of the partial K → P transformations during the heat treatment experiments since the actual size of the samples were small relative to the dimensions of the heating furnace and to the relevant temperature range. Also, as indicated earlier, our measurements revealed temperature homogeneity to within 5°C over the samples.

The weighing of some samples before and after the heat treatment did not reveal a correlation between the amount of evaporated material and the K → P phase transformation.

3.2.2. $TlMnCl_3$. The heat treatment experiments of different $TlMnCl_3$ samples revealed that the K → P phase transformation of this material can take place at temperatures as low as ~90°C. A complete transformation to the P phase occurred above 168°C, while between 89 and 144°C a partial K → P transformation was observed in two samples out of the five examined.

The results of the DSC analysis of four $TlMnCl_3$ samples are presented in Fig. 2. The observed thermal effects are listed below in two groups.

Group 1:															
I_a	135		153		165		180	203				(466)	(471)	(476)	491
II_a		142			162	177			220		330	Heating stopped at 386°C			
II_b											vvs	431 ?	(471) ?		498
III_a			157						225			Heating stopped at 386°C			
III_b														(487)	498
IV_a	135				160						332	Heating stopped at 371°C			
IV_b											330			(486)	503
Group 2:															
I_b		145 vvs								300		461			
II_c										302 vvs					498
III_c		145								301		461	471		
IV_c		145							247	302		461	471	479	

All the $TlMnCl_3$ samples initially contained both the K and the P phases. The occurrence of chemical reaction(s) was visually observed after the complete analyses of samples I, III, and IV, while no chemical reaction was visually observed after the three heating cycles of sample II and after the first heating cycle of sample III (the other samples were not visually examined after the first heating cycle).

Since no thermal effects were exhibited in the second heating cycles of samples II and III, except for the endothermic melting points at 498°C and an additional exothermic effect before the melting, it is possible to conclude that the K → P phase transformation of $TlMnCl_3$ is completed below 400°C and to assume that no thermal effects are exhibited on heating a cubic P $TlMnCl_3$ above room temperature. The experimental data also supports the assumption that the exothermic effects detected between 466 and 487°C before the first melting of the samples (first group I_a, II_b, III_b, and IV_b) and the thermal effects exhibited after this first melting (second group) are all con-

nected to chemical reaction(s) and to the product(s) of the chemical reaction(s). This assumption is also supported by the fact that no pronounced melting points are observed at 498°C after the first melting of the samples, except in the third heating cycle of sample II, where no chemical reaction could be visually observed. It should also be noted that this type of behavior was exhibited in a much more pronounced way by two $TlMnCl_3$ samples that were analyzed without being wrapped with gold foil (not shown in Fig. 2).

Because of the chemical reaction(s) that obviously occurred in the DSC experiments with $TlMnCl_3$ samples, it is not possible to correlate the different thermal effects to possible phase transformations and it is also possible that some of the effects are due to water vaporization. However, the other heat treatment experiments with $TlMnCl_3$ indicate that the K → P phase transformation of this material also proceeds in more than one pathway and probably at least some of the low-temperature ($t \leq 330$°C) thermal effects observed on the first heating cycles of $TlMnCl_3$ samples are related to this K → P phase transformation.

It is also logical to assume that the probability of a certain low-temperature ($t \leq 168$°C) K → P phase transformation pathway(s) is higher on a prolonged heating of the $TlMnCl_3$ samples, while the relatively faster heating rate (10°C/min) of the $TlMnCl_3$ samples during the DSC analyses reduced the probability of this low-temperature pathway(s) and raised the probability of other, higher-temperature (168°C $\leq t \leq$ 330°C) pathways. Therefore, it is possible that some of the thermal effects detected on the first heating cycles of the $TlMnCl_3$ DSC analyses at temperatures between 165 and 330°C are related to the K → P phase transformation even though the other heating experiments revealed a complete K → P phase transformation above 165°C.

4. Discussion

4.1. Discussion and Summary of the Data Relevant to the Phase Stabilities and Phase Transformations in $KMnCl_3$ and $TlMnCl_3$

The spontaneous, although sluggish, room-temperature transformation of the P phases of $KMnCl_3$ and $TlMnCl_3$ to their K phases reveals that at room temperature the more stable phases are the K phases and that the activation energy of the P → K phase transformation is relatively low.

The results of the heat treatment experiments indicate that the K → P phase transformation proceeds by more than one pathway. Although it is not yet possible to interpret the entirety of the results of the DSC analyses satisfactorily, it does seem that these results support the existence of more than one pathway for the K → P phase transformation.

No correlation was found through these experiments between the occurrence of the K phases and the existence of water (in amounts higher than 0.01%) in the crystal lattice, as was previously suggested (*4*). The assumption that no such correlation exists is supported by the results of the dehydration experiments of $KMnCl_3$ and of hydrated $TlMnCl_3$ and by the fact that the P → K spontaneous transformation also occurred in evacuated and sealed ampoules. A theoretical analysis that additionally supports this assumption is presented in Section 4.2.

Although the K phases of $KMnCl_3$ and $TlMnCl_3$ seem to be the more stable phases at room temperatures, the P phases of these materials retain their crystal structures for prolonged periods. While being crystallized in their P phases, $KMnCl_3$ and $TlMnCl_3$ pass through several crystallographic phase transformations which are reversible and temperature dependent; the highest temperature phase is the cubic P phase, which is further distorted into lower-symmetry

structures during the temperature lowering. This type of behavior is very common among compounds of the perovskite family and have been previously investigated both experimentally and theoretically (e.g., *20, 30, 31*). Two phase transformations were reported for $KCaCl_3$ and for $RbCaCl_3$ (*30*) and three phase transformation pathways were reported for $CsPbCl_3$ (*20*), $CsSrCl_3$ (*31*), and $TlMnCl_3$ (*20*).

The crystallographic changes occurring on cooling of P phase samples of $TlMnCl_3$ were investigated via X-ray, optical, and ultrasonic techniques and the following pathway was described (*20*) (the numbers in parentheses indicate the operations needed to derive the approximate unit cell parameters from the cubic phase):

$$\text{cubic, } Pm3m,\ z = 1 \xrightarrow{23^\circ C} \text{tetragonal,}$$

$$z = 1,\ (c/a) - 1 = \delta \xrightarrow{3^\circ C} \text{orthorhombic,}$$

$$z = 4,\ (2^{1/2}, 2, 2^{1/2}) \xrightarrow{-38^\circ C} \text{monoclinic}$$

(pseudoorthorhombic), $z = 8$, $(2^{1/2}, 2, 2 \cdot 2^{1/2})$.

For $KMnCl_3$ the present existing information reveals partial details on the following pathway:

$$\text{cubic, } Pm3m,\ z = 1 \xrightarrow{450^\circ C}$$

$$\text{phase II} \xrightarrow{386^\circ C} \text{phase III} \xrightarrow{255^\circ C}$$

orthorhombic, *Pnma*, $z = 4$, $(2^{1/2}, 2, 2^{1/2})$.

Aleksandrov's publication (*31*) suggests only one possible pathway for the distortions of a cubic P unit cell to the orthorhombic P *Pnma* one through three phase transformations. This suggestion implies that phase II is tetragonal, of the space group *I4/mcm* with $z = 4$ $(2^{1/2}, 2^{1/2}, 2)$, and that phase III is orthorhombic, *Cmcm*, with $z = 8$ (2, 2, 2). It would be of interest to investigate these high-temperature phases to support Aleksandrov's suggestion.

4.2. Theoretical Analysis

The occurrence of the $KCdCl_3$ structure in the $ABCl_3$ chlorides can be explained by the following analysis.

An ideal ABX_3 perovskite can be described as the stacking of close-packed (3-layered stacking = 3L) AX_3 layers, with the smaller *B* cations occupying octahedral interstices (e.g., *32*). The Goldsmidt geometrical tolerance factor (*32*) $t = r_A + r_X/2^{1/2}(r_B + r_X)$ then equals one. Geometrical and electrostatic considerations (e.g., *32*) show that when $t > 1$ a hexagonal stack of the close-packed layers enables larger dodecahedral coordinations for the relatively large *A* cations and that when $t < 1$, the *A* cation is too small for the dodecahedral coordination. Cooperative buckling of the octahedra, or small anion movements, lead, in these cases, to distorted perovskites. A review of all the existing information about ABF_3 and $ABCl_3$ compounds (*12, 24, 32, 33*) reveals that the fluoride group obeys the above-mentioned rules completely, while in the $ABCl_3$ group there are certain discrepancies (*24*). First, the hexagonal stacking of the ACl_3 layers starts at $t \simeq 0.93$ instead of at $t = 1$. This peculiarity of the chloride group is explained via the higher size and larger polarizability of the chloride ions (*9, 11, 12, 24, 33*). As was mentioned before, another peculiarity of the $ABCl_3$ group is that when $t \leq 0.93$, $KCdCl_3$ structures occur, as well as cubic and distorted perovskites. In any case, it is expected that when an only cubic (3L) stack exists, the perovskite distortions will increase with the size of the *B* cation and decrease with the size of the *A* cations. An analysis of the r^-/r^+ ratio of the different ions involved in the $ABCl_3$ compounds reveals that the geometry does not favor the close-packed ACl_3 layers required for the ideal 3L cubic perovskite structure. All *A* cations ($r_{Na} < r_A \leq r_{Cs}$) "prefer" a coordination of eight chlorine atoms [$r^-/r^+ \leq 1$ are

needed for a dodecahedral coordination around a cation, see, e.g., Ref. (*34*)]. It then follows that the existence of chloride perovskites could only be explained in terms of the high electrostatic energy gained by the BCl_6 octahedra and the assumption that the ACl_{12} dodecahedra are the unstable units in the structure. Calculations show that in an ideal perovskite, the contribution of the BX_6 octahedra to the electrostatic energy is 1.7 times greater than that of the ACl_{12} dodecahedra and that each B–X bond contributes approximately 3.5 times more to the electrostatic energy than an A–X bond.[1]

The Goldsmidt tolerance factor requires that in an ideal cubic perovskite, the relation $r_A + r_{Cl} = 2^{1/2}(r_B + r_{Cl})$ holds.

The higher these $r_A + r_{Cl}$ values are from the theoretical calculated ideal values, the more the structure will be distorted. In Table V, the known experimental B–Cl (B = Fe, Mn) and A–Cl (A = K, NH_4, Tl, Rb, Cs) distances of perovskite, hexagonal 2L, and K structure $ABCl_3$ compounds are listed, together with the theoretical calculated A–Cl distances and the lengthening of the experimental A–Cl distances relative to the calculated ones. The theoretical A–Cl distances were calculated as $r_A + r_{Cl} + 0.19$ when r_A and r_{Cl} are the appropriate Pauling's radii and 0.19 is a factor added for dodecahedral, rather than octahedral, coordination (*38*). The shortening of the Fe–Cl distances in the series of the hexagonal 2L compounds $NH_4FeCl_3 \rightarrow TlFeCl_3 \rightarrow RbFeCl_3 \rightarrow CsFeCl_3$ is expected from the decrease in the polarizing power of the relevant A cations and is also found in other $ABCl_3$ series (*24*). The data on the iron 2L compounds was added to Table V for the evaluation of the Fe–Cl distances expected for a hypothetical perovskite $KFeCl_3$.

It is possible to see from Table V that if $KMnCl_3$ and $KFeCl_3$ were to crystallize in a cubic P structure, the derived K–Cl distances would then be about 3.58 Å ($2^{1/2}$ 2.53, when 2.53 is the expected B–Cl distance for symmetrical $KBCl_3$ compounds of both cations, see Table V). This distance is about 0.25 Å greater than the theoretical

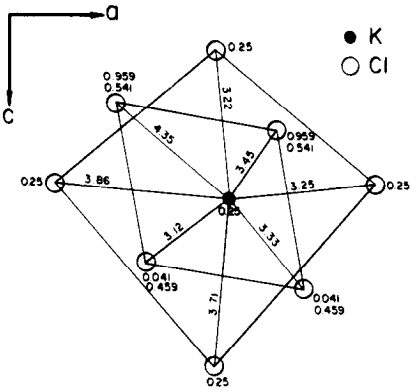

FIG. 3. The coordination around potassium in the orthorhombic perovskite $KMnCl_3$. An (010) projection. The numbers indicate distances (in Å) and heights of atoms (in fractions of the b parameter) along the b direction.

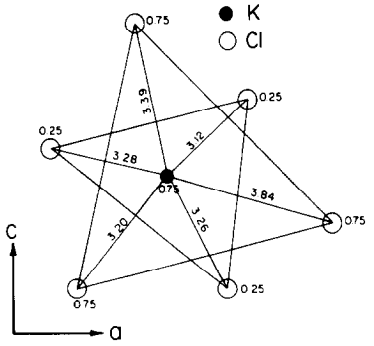

FIG. 4. The coordination around potassium in the $KCdCl_3$-type $KMnCl_3$. An (010) projection. The numbers indicate distances (in Å) and heights of atoms (in fractions of the b parameter) along the b direction.

[1] If a is the edge of the perovskite cube, than the electrostatic lattice energy gained by the nearest-neighbor attractions in the BCl_6 octahedra is $6\frac{e \cdot 2e}{0.5a} = 24e^2/a$ (when e is the electron charge) and the electrostatic energy due to the nearest-neighbor attractions in the ACl_{12} dodecahedra is $12\frac{e^2}{0.5\,3^{1/2}a} = 13.86e^2/a$.

TABLE V

DISTANCES IN PEROVSKITE (P), HEXAGONAL (2L), AND $KCdCl_3$ (K) STRUCTURES OF MANGANESE AND IRON $ABCl_3$ COMPOUNDS: EXPERIMENTAL B–Cl AND A—Cl DISTANCES, THEORETICAL CALCULATED A–Cl DISTANCES, AND THE LENGTHENING OF THE A–Cl DISTANCES (RELATIVE TO THE CALCULATED ONES, ALL DISTANCES IN Å)

Compound	Ref.	B–Cl distances	A–Cl distances	Theoretical calculated A–Cl distance	Lengthening of the actual A–Cl distance(s)	Compound	Ref.	B–Cl distances	A–Cl distances	Theoretical calculated A–Cl distance	Lengthening of the actual A–Cl distance(s)
$RbMnCl_3$ (cub P)	*6*	2.53	3.57	3.48	0.09	$KMnCl_3$(K)[a]	This work	2.42	3.12 × 2	3.33	−0.21
$TlMnCl_3$ (cub P)	*2*	2.51	3.55	3.44	0.11			2.54 × 2	3.20		−0.13
$TlMnCl_3$ (K)[a]	This work	2.43	3.21 × 2	3.44	−0.23			2.61 × 2	3.26 × 2		−0.07
		2.55 × 2	3.23 × 2		−0.21			2.64	3.28 × 2		−0.05
		2.68 × 2	3.24 × 2		−0.20				3.39		0.06
		2.81 × 2	3.26		−0.18				3.84		0.51
			3.58		0.14	$CsFeCl_3$ (2L)	*36*	2.47	3.63[c]	3.69	0.06
			3.84		0.40				3.68[d]		−0.01
NH_4MnCl_3 (cub P)	*35*	2.53	3.58	3.42	0.16	$RbFeCl_3$ (2L)	*36, 37*	2.48	3.54[c]	3.48	0.04
$KMnCl_3$ (orth P)[b]	This work	2.51 × 2	3.12 × 2	3.33	−0.21				3.64[d]		0.12
		2.53 × 2	3.25		−0.16	$TlFeCl_3$ (2L)	*2*	2.51	3.49[c]	3.44	0.05
		2.59 × 2	3.33 × 2		−0.08				3.62[d]		0.18
			3.45 × 2		−0.03	NH_4FeCl_3 (2L)	*35*	2.53	3.51[c]	3.42	0.09
			3.71		0.38				3.64[d]		0.22
			3.84		0.51	$KFeCl_3$ (K)[a]	*17*	2.49 × 2	3.21 × 2	3.33	−0.12
			3.86		0.53			2.58 × 2	3.22 × 2		−0.11
			4.35 × 2		1.02			2.501	3.24		−0.09
								2.499	3.30		−0.03
									3.39 × 2		0.06
									3.88		0.55

[a] For the geometrical distribution of the different chlorine atoms around the potassium ion in K $KMnCl_3$, see Fig. 2. The environment of the A cations in other K structure $ABCl_3$ compounds is similar.

[b] For the geometrical distribution of the different chlorine atoms around the potassium ion in P $KMnCl_3$, see Fig. 1.

[c] Distances to chlorine atoms in the same layer.

[d] Distances to chlorine atoms in an adjacent layer.

calculated value and obviously such a large A–Cl distance requires a strong distortion.

The distortions found for P $KMnCl_3$ (Table V and Fig. 3) reveal an asymmetrical coordination around the potassium cations so that the surrounding chlorine atoms are more concentrated on one side of the atom. Such asymmetry is created by the cooperative buckling of the coordination octahedra and is also found in the orthorhombic P structure of $KMgCl_3$ (*29*).

In the K structures of $KMnCl_3$, $TlMnCl_3$, and $KFeCl_3$, the coordination of the A cations is lower and also more regular in that the shorter and longer A–Cl bonds are more symmetrically distributed around the A cations (Table V and Fig. 4), although the coordination of the B cation is less symmetrical than it is in the perovskite compounds.

The conclusion from the above analysis is that the K ($KCdCl_3$) structure is more favorable than the P (perovskite) structure in $ABCl_3$ compounds for which the A–Cl distances derived from the expected cubic P structure is too long. Table V reveals that a lengthening of about 0.11 Å from the theoretical calculated values of the A–Cl distances is enough to stabilize the K structure (in $TlMnCl_3$). The lack of a K structure of NH_4MnCl_3 could only be explained via an assumption of strong hydrogen bonds that stabilize the cubic structure. However, there exists the possibility that a K structure might still be found for that compound.

The less symmetric coordination of the B cations in the K structure explains the relationship between this structure and the polarizability of the B cations (*5*, *12*).

It is also obvious that a polarizable anion is required for the K structure in ABX_3 compounds. This explains the absence of ABF_3 compounds with the K structure, even with the small sodium cations which "prefer" a coordination of eight fluorine anions, and leads to the expectation that this structure would be more common with ABX_3 bromides and iodides (higher polarizability and r^-/r^+ ratios). This expectation is

TABLE VI

DATA ON K STRUCTURES OF SOME ABX_3 BROMIDES AND IODIDES, COMPARED TO THE STRUCTURES OF THE PARALLEL CHLORIDE COMPOUNDS

Compound	Ref. to structural data	Structure (or nonexistence) of parallel chloride	Ref. to structural data on chloride
$TlMgBr_3$	*39*	Does not exist	*46* (No. 1342)
$KMgBr_3$	*39*	Orthorhombic P	*29*
$TlMnBr_3$	*40*	K and cubic P	This work
$KMnBr_3$	*41*	K and orthorhombic P	This work
$KFeBr_3$	*17*	K	*17*
$KCdBr_3$	*42*	K	*3*
$KCuBr_3$[a]	*16*	K[a]	*16*
$TlCuBr_3$[a]	*16*	K[a]	*16*
$KCrBr_3$[a]	*16*	K[a]	*16*
$TlCrBr_3$[a]	*16*	K[a]	*16*
$TlFeI_3$	*43*	2L hexagonal	*2*
$TlMnI_3$	*43*	K and cubic P	This work
$TlCdI_3$	*44*	Structure not known	
$KPbI_3$	*44*	Does not exist	*46* (No. 1269)
$RbPbI_3$	*44*	Tetragonal P	*47*
$CsPbI_3$	*45*	Orthorhombic P	*48*

[a] With additional cooperative Jahn–Teller distortions.

supported with recently accumulated data on bromides and iodides (*33*), the relevant details of which are presented in Table VI.

Acknowledgments

The authors would like to thank R. Reshef, E. Lichtenstein, and E. Levy for their technical assistance.

References

1. W. J. CROFT, M. KESTIGIAN, AND F. P. LEIPZIGER, *Inorg. Chem.* **4,** 423 (1965).
2. M. AMIT, A. ZODKEVITZ (HOROWITZ), AND J. MAKOVSKY, *Isr. J. Chem.* **8,** 737 (1970).
3. E. BRANDENBERGER, *Experimentia* **3,** 149 (1947).
4. P. BOHAC, A. GAUMANN, AND H. AREND, *Mater. Res. Bull.* **8,** 1299 (1973).
5. H. F. MCMURDIE, J. DEGROOT, M. MORRIS, AND H. E. SWANSON, *J. Res. Nat. Bur. Stand. Sect. A* **73,** 621 (1969).
6. J. M. LONGO AND J. A. KAFALAS, *J. Solid State Chem.* **3,** 429 (1971).
7. J. A. KAFALAS, J. M. LONGO, AND D. A. BATSON, *Solid State Res. Lincoln Lab. MIT* **2,** 36 (1970).
8. J. M. LONGO AND J. A. KAFALAS, *J. Solid State Chem.* **1,** 103 (1969).
9. T. I. LI, G. D. STUCKY, AND G. L. MCPHERSON, *Acta Crystallogr. Sect. B* **29,** 1330 (1973).
10. P. BOHAC, A. GÄUMANN, AND H. AREND, *Mater. Res. Bull.* **8,** 1299 (1973).
11. J. W. WEENK AND H. A. HARWIG, *J. Phys. Chem. Solids* **18,** 1055 (1977).
12. J. FERNANDEZ, M. J. TELLO, AND M. A. ARRIANDIAGA, *Mater. Res. Bull.* **13,** 477 (1978).
13. C. H. MACGILLVAVEY, H. NIJVELD, S. DIERDORP, AND J. KARSTEN, *Rec. Trav. Chim. Pays-Bas* **58,** 193 (1939).
14. J. HUART, *Bull. Soc. Fr. Mineral. Cristallogr.* **88,** 65 (1965).
15. V. A. WEISS AND K. Z. DAMM, *Z. Naturforsch. B* **9,** 82 (1954).
16. W. J. CRAMA, Thesis, Leiden (1980).
17. J. MAKOVSKY, A. HOROWITZ (ZODKEVITZ), AND M. AMIT, *Isr. J. Chem.* **12,** 827 (1974).
18. H. J. SEIFERT AND F. W. KOKNAT, *Z. Anorg. Allg. Chem.* **341,** 269 (1965). [German]
19. M. KESTIGIAN, *Mater. Res. Bull.* **5,** 263 (1970).
20. A. T. ANISTRATOV, A. I. KRUPNYI, L. A. POZDNYAKOVA, S. V. MELNIKOVA, AND B. V. BEZNOSIKOV, *Sov. Phys. Solid State* **17,** 471 (1975).
21. E. R. NATSVLISHVILI AND A. G. BERGMAN, *Zh. Obsch. Khim.* **9**(7), 644 (1939). [Russian]
22. E. GUREWITZ, A. HOROWITZ, AND H. SHAKED, *Phys. Rev. B* **20,** 4544 (1979).
23. E. GUREWITZ, M. MELAMUD, A. HOROWITZ, AND H. SHAKED, *Phys. Rev. B,* in press.
24. A. HOROWITZ, Ph.D. thesis, The Hebrew University of Jerusalem (1981).
25. S. J. JENSEN, *Acta Crystallogr. Sect. A* **21,** 56 (1966) (suppl.).
26. M. AMIT, private communication.
27. H. P. HANSON, F. HERMAN, J. D. LEA, AND S. SKILLMAN, *Acta Crystallogr.* **17,** 1040 (1964).
28. J. S. ROLLET, "Computing Methods in Crystallography," pp. 52–56, Pergamon, New York (1965).
29. J. BRYNESTAD, H. L. YAKEL, AND G. P. SMITH, *J. Chem. Phys.* **45,** 4652 (1966).
30. M. MIDORIKAWA, Y. ISHIBASHI, AND Y. TAKAGI, *J. Phys. Japan* **46,** 1240 (1979).
31. K. S. ALEKSANDROV, *Sov. Phys. Crystallogr.* **21,** 133 (1976).
32. J. B. GOODENOUGH AND J. M. LONGO, "Ländolt–Böernstein, Numerical Data and Functional Relationships in Science and Technology, New Series, Group III: Crystal and Solid State Physics," Vol. 4, Magnetic and Other Properties of Oxides and Related Compounds" (K. H. Hellwege and A. M. Hellwege, Eds.), Chap. 3, p. 126, Springer-Verlag, Berlin/New York (1970).
33. A. HOROWITZ, to be published *in* "Progress in Inorganic Chemistry," Wiley, New York.
34. F. A. COTTON AND G. WILKINSON, "Advanced Inorganic Chemistry," 2nd ed., p. 47, Interscience, London (1966).
35. M. AMIT, A. ZODKEVITZ, AND J. MAKOVSKY, *Isr. J. Chem.* **8,** 737 (1970).
36. H. J. SEIFERT AND K. KLATYK, *Z. Anorg. Allg. Chem.* **342,** 1 (1966).
37. N. ACHIVA, *J. Phys. Soc. Japan* **27,** 561 (1969).
38. M. SCHIEBER, "Introduction to Physical Metallurgy and Ceramics, Part I—Solid State Chemical Principles," p. 26, Academon—The Hebrew University, Jerusalem (1970).
39. H. J. SEIFERT AND J. WASEL-NIELEN, *Rev. Chim. Mineral.* **14,** 503 (1977).
40. H. J. SEIFERT, T. KRIMMEL, AND W. J. HEINEMANN, *Thermal Anal.* **6,** 175 (1974).
41. H. J. SEIFERT AND G. FLOHR, *Z. Anorg. Allg. Chem.* **436,** 244 (1977).
42. D. E. HOLMES, M. L. HARVILL, AND L. D. BOGAN, *Mater. Res. Bull.* **10,** 753 (1975).
43. H. W. ZANDBERGEN, *J. Solid State Chem.* **37,** 308 (1981).
44. H. W. ZANDBERGEN, *J. Solid State Chem.* **37,** 189 (1981).
45. C. K. MØLLER, *Mat. Fys. Medd. Dan. Vid. Selsk.*

32, No. 2 (1959).
46. E. M. LEVIN, C. R. ROBINS, AND H. MCMURDIE, "Phase Diagrams for Ceramists," Vol. 1 (1964), Vol. 2 (1969), and Vol. 3 (1975), The American Ceramic Society, Columbus, Ohio.
47. G. J. GANZ, "Molten Salts Handbook," p. 157, Academic Press, New York (1967).
48. S. HIROTSU, *J. Phys. Soc. Japan* **31,** 552 (1971).